Generation of nonreciprocal single photons in the chiral waveguide-cavity-emitter system

Wen-ju Gu,* Lei Wang, Zhen Yi,† and Li-hui Sun
School of Physics and Optoelectronic Engineering, Yangtze University, Jingzhou 434023, China

(Received 23 March 2022; accepted 10 October 2022; published 28 October 2022)

We investigate the generation of nonreciprocal single photons in the chiral waveguide-cavity-emitter system. Due to the chirality of light-emitter interactions, photons in the left direction couple to a cavity which induces only linear optical effects, while photons in the right direction couple to a cavity-emitter system which can generate optical nonlinearity. In the regime of single-photon transmission, photons in the left direction are absorbed by the cavity at the resonance frequency, while photons in the right direction are transmitted due to the Rabi splitting. In the regime of two-photon transmission, optical linearity in the left direction cannot produce photon-photon interactions and does not change the statistics of photons. However, the effective repulsive interaction between photons can be produced by the optical nonlinearity in the right direction, suppressing two-photon transmission (photon blockade). Physically, the photon-photon bound state, which emerges due to the strong-photon-photon correlation mediated by the cavity-emitter system, plays a key role in generation of photon blockade at the resonance frequency. As a result, nonreciprocal single photons can be realized in the combination of single-photon transmission and photon blockade at the resonance frequency. Additionally, photon-photon interactions are sensitive to the width of the wave packet since photons should coincide at the interaction site.

DOI: 10.1103/PhysRevA.106.043722

I. INTRODUCTION

With the development of quantum technologies in the emerging field of waveguide quantum electrodynamics (WQED), various experimental platforms offer the intriguing possibility to realize the coupling between quantum emitters (QEs) and propagating photons through the integration of natural or artificial atoms, such as superconducting qubits and solid-state quantum dots and defects, and different types of optical and microwave waveguides [1–3]. The research offers novel opportunities both for fundamental physics and for quantum information processing (QIP) [4]. The spatial confinement of light leads to stronger light-QE interactions in WQED, which enables the realization of near-deterministic and coherent interfaces [5,6]. In particular, the tight light confinement within advanced photonic nanostructures brings about a new chiral interface, where the light-QE interaction relies on the propagation direction of light and the polarization of the transition dipole moment of the QE [7–11]. This type of chiral interaction constitutes a new element of the quantum optics toolbox and opens up a range of nontrivial functionalities and applications. It has motivated a number of proposals of nonreciprocal devices in the quantum regime, such as optical circulators and switches at a single-photon level [12–14], non-destructive photon detectors [15], implementation of $\sqrt{\text{SWAP}}$ gates [16], and the deterministic photonic Duan-Kimble quantum gate [17]. In order to operate better at the single-photon level, researchers have recently investigated an alternative cavity-based chiral quantum interface where cavities are employed to enhance the coupling between light and QEs and also effectively increase the optical nonlinearities [18–21].

The cavity-based chiral quantum interface requires the use of nontransversally polarized whispering gallery mode (WGM) resonators such as bottle, disk, sphere, and ring microstructures [20–23]. Counterpropagating photons are distinguishable by their nearly orthogonal polarizations, which are almost perfectly circularly polarized in the plane of propagation with the input of linearly polarized pump light. When a circularly polarized QE lies near the resonator, nonreciprocal transmissions at the single-photon level have been exhibited [21]. Moreover, the strong coupling of QE and cavities gives rise to optical nonlinearity at the level of individual quanta. The realization of coherent interactions between individual photons could enable a wide variety of scientific and engineering applications in the regime of quantum nonlinear optics [24]. Furthermore, the few-photon quantum effects observed in recent experimental systems have sparked extensive interest in the many-body problem of light propagation in strongly nonlinear media [25].

In this work, we investigate the nonreciprocal single-photon and two-photon transmissions in the chiral waveguide-cavity-QE system. For the single-photon dynamics, the photon in the right propagation direction enables the cavity-QE interaction. It leads to the transmission on resonance with the cavity frequency due to well-known vacuum-Rabi splitting [26]. However, the left-moving photon couples to only the cavity, and the transmission is suppressed due to the absorption at the resonance frequency. Furthermore, in the two-photon dynamics, quantum nonlinearity induced by

*guwenju@yangtzeu.edu.cn
†yizhen@yangtzeu.edu.cn

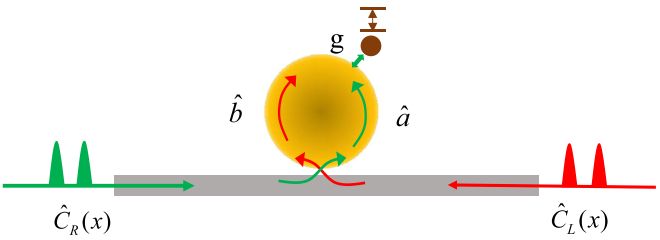

FIG. 1. Schematic of chiral coupling in the waveguide-cavity-QE system. A microcavity simultaneously couples to a nearby waveguide and a single two-level QE. The light propagating in the $+x$ ($-x$) direction drives the counterclockwise (clockwise) mode. The polarization of the evanescent field of the counterclockwise mode is σ^+ polarized outside the cavity wall, while that for the clockwise mode is σ^- polarized. The transition of the two-level QE is σ^+ polarized.

resonator-QE interactions can produce repulsion or attraction between photons [27–31]. Thus, photon blockade and photon-induced tunneling are tunable in the right direction. In such a system, strong photon blockade is achievable in addition to the single-photon transmission at the resonance frequency, enabling the capability to generate single photons on demand. In contrast, since the cavity servers as a linear system in the left direction, photon-photon interactions are impossible. The photon statistics remains unchanged.

This paper is organized as follows. In Sec. II, the chiral waveguide-cavity-QE system is introduced, and nonreciprocal transmissions of single- and two-photon incident states are analyzed in Secs. III and IV. In Sec. V, the nonreciprocal photon blockade is discussed, and finally, the conclusions are drawn in Sec. VI.

II. CHIRAL COUPLINGS IN THE WAVEGUIDE-CAVITY-QE SYSTEM

We consider a waveguide-cavity-QE system in which a microcavity couples to both a nearby waveguide and a two-level QE, as shown in Fig. 1. The right-propagating light in the $+x$ direction of the waveguide drives the counterclockwise (CCW) mode in the microcavity, and the left-propagating light in the $-x$ direction drives the clockwise (CW) mode. The polarization of the evanescent field of the CCW mode is σ^+ polarized outside the cavity wall, while that for the CW mode is σ^- polarized [21]. Here we suppose that the dipole transition of a two-level QE is σ^+ polarized. Thus, the CCW mode couples to the emitter, whereas the CW mode decouples from it. The system is described by the Hamiltonian ($\hbar = 1$)

$$\begin{aligned}\hat{H} =& \int dx[\hat{c}_R^\dagger(x)(\omega_0 - iv_g\partial_x)\hat{c}_R(x) + \hat{c}_L^\dagger(x)(\omega_0 + iv_g\partial_x)\hat{c}_L(x)] \\ &+ (\omega_c - i\kappa/2)(\hat{a}^\dagger\hat{a} + \hat{b}^\dagger\hat{b}) + (\omega_{eg} - i\gamma/2)\hat{\sigma}_{ee} \\ &+ \frac{V}{2}\int dx\delta(x)[\hat{c}_R^\dagger(x)\hat{a} + \hat{a}^\dagger\hat{c}_R(x) + \hat{c}_L^\dagger(x)\hat{b} + \hat{b}^\dagger\hat{c}_L(x)] \\ &+ \frac{g}{2}(\hat{a}^\dagger\hat{\sigma}_{ge} + \hat{\sigma}_{eg}\hat{a}), \end{aligned} \tag{1}$$

where $\hat{c}_R^\dagger(x)$ and $\hat{c}_L^\dagger(x)$ are the creation operators of right- and left-propagating photons in real space and $\hat{a}^\dagger$ and $\hat{b}^\dagger$ are the creation operators of CCW and CW cavity modes with the same frequency ω_c and damping rate κ. Here ω_0 can be an arbitrary frequency that is away from the cutoff frequency of the photonic waveguide, and v_g is the group velocity [32]. The atomic transition frequency and dissipation rate are ω_{eg} and γ, respectively, and the atomic operator is $\hat{\sigma}_{mn} = |m\rangle\langle n|$ $(m, n) = (e, g)$. The waveguide-cavity and cavity-QE coupling strengths are V and g, respectively. Here we take the $\delta(x)$ function to describe the form of the interaction between the waveguide and the microcavity, as in previous works [32,33]. This model is valid under the assumption of the Markovian approximation [34], in which the strength between the waveguide and the cavity is independent of k. In experiment, it requires the transversal scale of the cavity to be much narrower than the wavelength of the guided light. In contrast, non-δ coupling should be considered when the transversal scale of the cavity is comparable with or larger than the wavelength of the guided light [35]. Then we introduce a free Hamiltonian

$$\begin{aligned}\hat{H}_0 =& \omega_0\int dx[\hat{c}_R^\dagger(x)\hat{c}_R(x) + \hat{c}_L^\dagger(x)\hat{c}_L(x)] \\ &+ \omega_0(\hat{\sigma}_{ee} + \hat{a}^\dagger\hat{a} + \hat{b}^\dagger\hat{b}) \end{aligned} \tag{2}$$

and an unitary operator $\hat{U}(t) = \exp(-i\hat{H}_0 t)$, and the Hamiltonian is transformed into the interaction picture following the relation

$$\hat{H}_I = \hat{U}^\dagger(t)\hat{H}\hat{U}(t) + i[\partial_t\hat{U}^\dagger(t)]\hat{U}(t). \tag{3}$$

In the interaction picture, the Hamiltonian can be split into two parts to describe right- and left-moving modes, respectively,

$$\begin{aligned}\hat{H}_I =& \hat{H}_R + \hat{H}_L, \\ \hat{H}_R =& \tilde{\Delta}_c\hat{a}^\dagger\hat{a} - iv_g\int dx\hat{c}_R^\dagger(x)\partial_x\hat{c}_R(x) + \tilde{\Delta}_e\hat{\sigma}_{ee} \\ &+ \frac{V}{2}\int dx\delta(x)[\hat{c}_R^\dagger(x)\hat{a} + \hat{a}^\dagger\hat{c}_R(x)] + \frac{g}{2}(\hat{a}^\dagger\hat{\sigma}_{ge} + \hat{\sigma}_{eg}\hat{a}), \\ \hat{H}_L =& \tilde{\Delta}_c\hat{b}^\dagger\hat{b} + iv_g\int dx\hat{c}_L^\dagger(x)\partial_x\hat{c}_L(x) \\ &+ \frac{V}{2}\int dx\delta(x)[\hat{c}_L^\dagger(x)\hat{b} + \hat{b}^\dagger\hat{c}_L(x)]. \end{aligned} \tag{4}$$

Here $\tilde{\Delta}_c = \Delta_c - i\kappa/2$ and $\tilde{\Delta}_e = \Delta_e - i\gamma/2$ are the complex detunings, with $\Delta_c = \omega_c - \omega_0$ and $\Delta_e = \omega_{eg} - \omega_0$. For simplicity, we will take v_g to be 1 hereafter.

III. NONRECIPROCAL TRANSMISSIONS OF THE SINGLE-PHOTON INPUT STATES

We first consider the single-photon scattering processes, where the incident states in the left- and right-propagating channels are confined within one excitation. In the left-propagating subspace, the scattering eigenstate is given by

$$|\Psi_1\rangle_L = \int dx f_{k_1}^{(L)}(x)\hat{c}_L^\dagger(x)|0_L, 0_b\rangle + h_b|0_L, 1_b\rangle, \tag{5}$$

where $|0_L, 0_b\rangle$ is the vacuum state of left-propagating waveguide and cavity modes and $|0_L, 1_b\rangle$ is the vacuum state of the waveguide mode with one excitation in the cavity mode. From

the equation $\hat{H}_L|\Psi_1\rangle_L = E_1|\Psi_1\rangle_L$, with eigenvalue $E_1 = k_1$, we can obtain

$$(i\partial_x - k_1)f_{k_1}^{(L)}(x) + \frac{V}{2}h_b\delta(x) = 0,$$
$$(\tilde{\Delta}_c - k_1)h_b + \frac{V}{2}f_{k_1}^{(L)}(0) = 0. \tag{6}$$

Here the function $f_{k_1}^{(L)}(x)$ is piecewise continuous because of the singularity of the δ function [36], and $f_{k_1}^{(L)}(0) \equiv [f_{k_1}^{(L)}(0^+) + f_{k_1}^{(L)}(0^-)]/2$. By eliminating h_b and employing the continuity condition at $x = 0$, where the interaction occurs, we have

$$f_{k_1}^{(L)}(0^-) = t_{k_1}^{(\mathrm{L})} f_{k_1}^{(L)}(0^+),$$
$$t_{k_1}^{(\mathrm{L})} = \frac{\tilde{\Delta}_c - k_1 + i\Gamma/2}{\tilde{\Delta}_c - k_1 - i\Gamma/2}, \tag{7}$$

where $\Gamma = V^2/4$ indicates the coupling rate between the cavity and the one-dimensional (1D) continuum and $t_{k_1}^{(\mathrm{L})}$ is the transmission amplitude of the left-propagating incident photon. For $x > 0$, the incident state is a plane wave before interaction,

$$|k_1\rangle_L = \int dx h_{k_1}^{(\mathrm{L})}(x)\hat{c}_L^\dagger(x)|0_L, 0_b\rangle, \tag{8}$$

with $h_{k_1}^{(\mathrm{L})}(x) = \langle x|k_1\rangle = e^{-ik_1x}/\sqrt{2\pi}$. Thus, $f_{k_1}^{(L)}(0^+) = h_{k_1}^{(\mathrm{L})}(0) = 1/\sqrt{2\pi}$, and according to the continuity condition, the wave function becomes $f_{k_1}^{(L)}(x) = t_{k_1}^{(\mathrm{L})}h_{k_1}^{(\mathrm{L})}(x)$ for $x < 0$. In reality, the far-field approximation should be satisfied, i.e., x much larger than the size of the cavity mode. In total, the wave function can be written as

$$f_{k_1}^{(L)}(x) = h_{k_1}^{(\mathrm{L})}(x)\big[\theta(x) + t_{k_1}^{(\mathrm{L})}\theta(-x)\big] \tag{9}$$

with the use of the Heaviside step function $\theta(x)$.

Similarly, the scattering eigenstate in the right-propagating subspace is given by

$$|\Psi_1\rangle_R = \int dx f_{k_1}^{(R)}(x)\hat{c}_R^\dagger(x)|0_R, 0_a, g\rangle + h_a|0_R, 1_a, g\rangle + h_e|0_R, 0_a, e\rangle, \tag{10}$$

where $|0_R, 0_a, g\rangle$ is the vacuum state of the right-propagating waveguide and cavity modes with the QE in its ground state, $|0_R, 1_a, g\rangle$ is one excitation in the cavity mode, and $|0_R, 0_a, e\rangle$ is one excitation in the QE. From the equation $\hat{H}_R|\Psi_1\rangle_R = E_1|\Psi_1\rangle_R$, with eigenvalue $E_1 = k_1$, we can obtain

$$(-i\partial_x - k_1)f_{k_1}^{(R)}(x) + \frac{V}{2}h_a\delta(x) = 0,$$
$$(\tilde{\Delta}_c - k_1)h_a + \frac{V}{2}f_{k_1}^{(R)}(0) + \frac{g}{2}h_e = 0, \tag{11}$$
$$(\tilde{\Delta}_e - k_1)h_e + \frac{g}{2}h_a = 0.$$

Here $f_{k_1}^{(R)}(x)$ is also piecewise continuous, with $f_{k_1}^{(R)}(0) \equiv [f_{k_1}^{(R)}(0^+) + f_{k_1}^{(R)}(0^-)]/2$. By eliminating h_a and h_e, the continuity condition becomes

$$f_{k_1}^{(R)}(0^+) = t_{k_1}^{(\mathrm{R})} f_{k_1}^{(R)}(0^-),$$
$$t_{k_1}^{(\mathrm{R})} = \frac{(\tilde{\Delta}_c - k_1 + i\Gamma/2)(\tilde{\Delta}_e - k_1) - g^2/4}{(\tilde{\Delta}_c - k_1 - i\Gamma/2)(\tilde{\Delta}_e - k_1) - g^2/4}, \tag{12}$$

where $t_{k_1}^{(\mathrm{R})}$ is the transmission amplitude for the right-propagating mode. For $x < 0$, with the incident plane-wave state

$$|k_1\rangle_R = \int dx h_{k_1}^{(\mathrm{R})}(x)\hat{c}_R^\dagger(x)|0_R, 0_a, g\rangle \tag{13}$$

and $h_{k_1}^{(\mathrm{R})}(x) = e^{ik_1x}/\sqrt{2\pi}$, the wave function becomes $f_{k_1}^{(R)}(x) = t_{k_1}^{(\mathrm{R})}h_{k_1}^{(\mathrm{R})}(x)$ for $x > 0$. Thus, the total wave function can be written as

$$f_{k_1}^{(R)}(x) = h_{k_1}^{(\mathrm{R})}(x)\big[\theta(-x) + t_{k_1}^{(\mathrm{R})}\theta(x)\big]. \tag{14}$$

We suppose that the incident single-photon pulses are described by wave packets

$$\big|\psi_j^{(1)}\big\rangle = \int dk\alpha(k)|k\rangle_j \quad (j = R, L), \tag{15}$$

with the Gaussian-type spectral amplitude

$$\alpha(k) = \frac{1}{(2\pi\sigma^2)^{1/4}}\exp\left[-\frac{(k-k_0)^2}{4\sigma^2}\right]. \tag{16}$$

Here σ is the width, and k_0 corresponds to the central frequency. The single-photon transmitted states are $|\varphi_j^{(1)}\rangle = \int dk\alpha(k)t_k^{(j)}|k\rangle_j$, and the transmission probabilities are given by

$$T_L = \int dk_1 \big|_L\langle k_1|\varphi_L^{(1)}\rangle\big|^2 = \int dk_1\alpha^2(k_1)\big|t_{k_1}^{(\mathrm{L})}\big|^2,$$
$$T_R = \int dk_1 \big|_R\langle k_1|\varphi_R^{(1)}\rangle\big|^2 = \int dk_1\alpha^2(k_1)\big|t_{k_1}^{(\mathrm{R})}\big|^2. \tag{17}$$

To evaluate the nonreciprocal single-photon transmission properties, we numerically calculate transmission probabilities of left- and right-propagating lights as a function of detuning $\Delta_k = k_0 - \omega_0$ in Fig. 2. We follow the parameters taken in the experimental platforms composed of a single ^{85}Rb atom strongly coupled to a WGM bottle microresonator [19,21]. Meanwhile, the microresonator couples to a tapered fiber with near-lossless in- and out-coupling of light. The atom-light coupling strength is about $g/2\pi = 20$ MHz, and the cavity decay rate $\kappa/2\pi = 10$ MHz, with the decay rate of the atomic transition being on the scale of megahertz. In calculations, we take $\Delta_c = 0$, $\Delta_e = 0$, $g = 2\kappa$, $\Gamma = 4\kappa$, and $\gamma = 0.1\kappa$. In the right direction, the cavity-QE interaction produces the vacuum-Rabi splitting at resonance frequency with $\Delta_k = \pm g/2$. When the central frequency k_0 is positioned between the splittings, the transmission probability shows a sharp peak at $\Delta_k = 0$, originating from the destructive interference

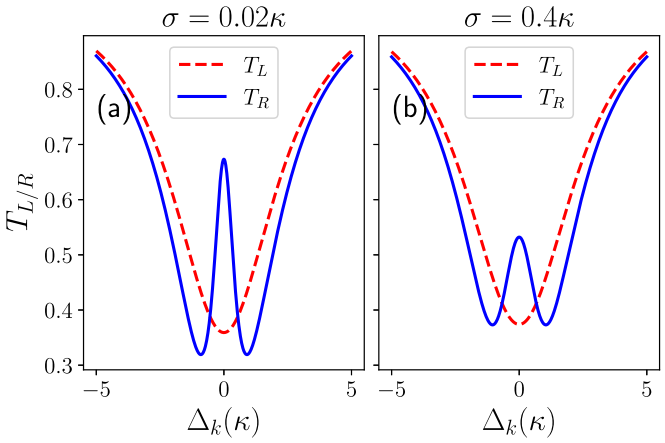

FIG. 2. Single-photon transmission probabilities in the chiral waveguide-cavity-QE system as a function of Δ_k (in units of κ) with the spectral widths (a) $\sigma = 0.02\kappa$ and (b) $\sigma = 0.4\kappa$. Dashed lines indicate probabilities of left-propagating light, and solid lines indicate probabilities of right-propagating light. The other parameters are $\Delta_c = 0$, $\Delta_e = 0$, $g = 2\kappa$, $\gamma = 0.1\kappa$, and $\Gamma = 4\kappa$.

between two dressed states [21]. This electromagnetically-induced-transparency-like effect has been investigated in the system that consists of a flying optical photon interacting with Fabry-Pérot optical cavities in the presence or absence of a resonant two-level medium to realize photonic controlled-phase gates [37–41]. In Fig. 2, the height of the central peak is $|\frac{\gamma(\kappa-\Gamma)+g^2}{\gamma(\kappa+\Gamma)+g^2}|^2$ in the narrow-bandwidth limit, whereas the height begins to get suppressed when σ becomes comparable with the width of the window $[\sim g^2/(\Gamma+\kappa)]$, as seen from Eq. (12). In comparison, left-propagating photons are absorbed by the cavity at $\Delta_k = 0$, and the absorption width is $\sim\kappa + \Gamma$, as seen from Eq. (7). Therefore, the shape of transmission lines is insensitive to a spectral width σ from 0.02 to 0.4, which is much smaller than $\kappa + \Gamma$.

IV. TRANSMISSIONS OF THE TWO-PHOTON PULSES

A. Scattering eigenstates within the left-propagating two-excitation subspace

We further consider two-photon scattering processes. In the left direction, the scattering eigenstate within the two-excitation subspace is

$$|\Psi_2\rangle_L = \iint dx_1 dx_2 f_2(x_1,x_2)\hat{c}_L^\dagger(x_1)\hat{c}_L^\dagger(x_2)|0_L,0_b\rangle + \int dx_1 f_b(x_1)\hat{c}_L^\dagger(x_1)|0_L,1_b\rangle + h_b|0_L,2_b\rangle. \quad (18)$$

The function $f_2(x_1,x_2)$ is the probability amplitude of two photons in the waveguide mode, which is symmetric due to the bosonic statistics, i.e., $f_2(x_1,x_2) = f_2(x_2,x_1)$. Moreover, $f_b(x_1)$ is the probability amplitude of having one photon in the waveguide mode with the other excitation in the cavity mode, and h_b is the probability amplitude of both excitations being in the cavity mode. From the equation $\hat{H}_L|\Psi_2\rangle_L = E_2|\Psi_2\rangle_L$, with

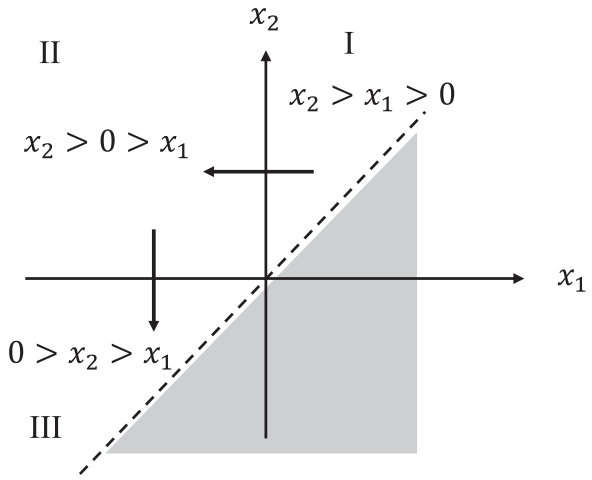

FIG. 3. The $x_2 > x_1$ region is dissected into three subregions, (I) $x_2 > x_1 > 0$, (II) $x_2 > 0 > x_1$, and (III) $0 > x_2 > x_1$, due to interactions at the coordinate axes $x_1 = 0$ and $x_2 = 0$.

the eigenvalue $E_2 = k_1 + k_2$, we can obtain

$$\begin{aligned}
&\left[i\left(\partial_{x_1}+\partial_{x_2}\right) - E_2\right]f_2(x_1,x_2) \\
&\quad + \frac{V}{4}[\delta(x_1)f_b(x_2) + \delta(x_2)f_b(x_1)] = 0, \\
&\left(i\partial_{x_1} - E_2 + \tilde{\Delta}_c\right)f_b(x_1) + \frac{V}{\sqrt{2}}h_b\delta(x_1) \\
&\quad + \frac{V}{2}[f_2(0,x_1) + f_2(x_1,0)] = 0, \\
&(2\tilde{\Delta}_c - E_2)h_b + \frac{V}{\sqrt{2}}f_b(0) = 0.
\end{aligned} \quad (19)$$

Here both functions $f_2(x_1,x_2)$ and $f_b(x_1)$ are piecewise continuous because of the singularity of the δ function, and $f_2(0,x_1) \equiv [f_2(0^+,x_1) + f_2(0^-,x_1)]/2$, $f_2(x_1,0) \equiv [f_2(x_1,0^+) + f_2(x_1,0^-)]/2$, and $f_b(0) \equiv [f_b(0^+) + f_b(0^-)]/2$. Since waveguide-cavity interactions occur at the coordinate axes $x_1 = 0$ and $x_2 = 0$ in real space, for the region of $x_1 \neq 0$ and $x_2 \neq 0$ in the absence of interactions, $f_2(x_1,x_2)$ yields

$$\left[i\left(\partial_{x_1}+\partial_{x_2}\right) - E_2\right]f_2(x_1,x_2) = 0. \quad (20)$$

The continuity conditions are necessary to calculate $f_2(x_1,x_2)$ and $f_b(x_1)$. For $f_b(x_1)$, the continuity condition becomes $f_b(0^-) = \eta_L(E_2)f_b(0^+)$ after eliminating h_b in Eqs. (19), where

$$\eta_L(E_2) = \frac{2\tilde{\Delta}_c - E_2 + i\Gamma}{2\tilde{\Delta}_c - E_2 - i\Gamma}. \quad (21)$$

For $f_2(x_1,x_2)$, it is convenient to consider the half-space $x_2 > x_1$ and then extend it to the full space through bosonic symmetry. In this case, the $x_2 > x_1$ region is dissected by the x_1 and x_2 axes into three subregions: (I) $x_2 > x_1 > 0$, (II) $x_2 > 0 > x_1$, and (III) $0 > x_2 > x_1$, as shown in Fig. 3. In subregion I, it corresponds to an incident plane-wave state before interactions, which is described by $f_2^{(\mathrm{I})}(x_1,x_2) = [h_{k_1}^{(\mathrm{L})}(x_1)h_{k_2}^{(\mathrm{L})}(x_2) + h_{k_1}^{(\mathrm{L})}(x_2)h_{k_2}^{(\mathrm{L})}(x_1)]/2$.

Through the integration of Eqs. (19) around the boundary between subregions I and II at $x_1 = 0$, we have

$$\begin{aligned} &i\big[f_2^{(\mathrm{I})}(0^+, x_2) - f_2^{(\mathrm{II})}(0^-, x_2)\big] + \frac{V}{4} f_b(x_2) = 0, \\ &\big(i\partial_{x_2} - E_2 + \tilde{\Delta}_c\big) f_b(x_2) + \frac{V}{2}\big[f_2^{(\mathrm{I})}(0^+, x_2) \\ &\quad + f_2^{(\mathrm{II})}(0^-, x_2)\big] = 0. \end{aligned} \tag{22}$$

Then by further eliminating $f_b(x_2)$, it becomes

$$\begin{aligned} &\big(i\partial_{x_2} - E_2 + \tilde{\Delta}_c - i\Gamma/2\big) f_2^{(\mathrm{II})}(0^-, x_2) \\ &\quad = \big(i\partial_{x_2} - E_2 + \tilde{\Delta}_c + i\Gamma/2\big) f_2^{(\mathrm{I})}(0^+, x_2). \end{aligned} \tag{23}$$

Because $f_2^{(\mathrm{I})}(0^+, x_2) = (e^{-ik_2 x_2} + e^{-ik_1 x_2})/4\pi$ on the boundary of subregion I, on the boundary of subregion II

$$\begin{aligned} f_2^{(\mathrm{II})}(0^-, x_2) = \frac{1}{4\pi}\big(t_{k_2}^{(\mathrm{L})} e^{-ik_1 x_2} + t_{k_1}^{(\mathrm{L})} e^{-ik_2 x_2}\big) \\ + A e^{(i\tilde{\Delta}_c - iE_2 + \Gamma/2)x_2}. \end{aligned} \tag{24}$$

We should take the coefficient A to be zero due to the divergence of the $e^{\Gamma x_2/2}$ term in the limit $x_2 \to \infty$. With the use of the equation $[i(\partial_{x_1} + \partial_{x_2}) - E_2] f_2^{(\mathrm{II})}(x_1, x_2) = 0$ in subregion II, $f_2^{(\mathrm{II})}(x_1, x_2)$ becomes

$$f_2^{(\mathrm{II})}(x_1, x_2) = \frac{1}{4\pi}\big(t_{k_2}^{(\mathrm{L})} e^{-ik_1 x_2 - ik_2 x_1} + t_{k_1}^{(\mathrm{L})} e^{-ik_1 x_1 - ik_2 x_2}\big). \tag{25}$$

Following the same procedure through the integration of Eqs. (19) around the boundary between subregion II and subregion III ($x_2 = 0$), we have

$$\begin{aligned} &\big(i\partial_{x_1} - E_2 + \tilde{\Delta}_c - i\Gamma/2\big) f_2^{(\mathrm{III})}(x_1, 0^-) \\ &\quad = \big(i\partial_{x_1} - E_2 + \tilde{\Delta}_c + i\Gamma/2\big) f_2^{(\mathrm{II})}(x_1, 0^+). \end{aligned} \tag{26}$$

Since $f_2^{(\mathrm{II})}(x_1, 0^+) = (t_{k_2}^{(\mathrm{L})} e^{-ik_2 x_1} + t_{k_1}^{(\mathrm{L})} e^{-ik_1 x_1})/4\pi$, we have

$$\begin{aligned} f_2^{(\mathrm{III})}(x_1, 0^-) = \frac{1}{4\pi} t_{k_1}^{(\mathrm{L})} t_{k_2}^{(\mathrm{L})} (e^{-ik_1 x_1} + e^{-ik_2 x_1}) \\ + B e^{(i\tilde{\Delta}_c - iE_2 + \Gamma/2)x_1}. \end{aligned} \tag{27}$$

The coefficient B is determined by the continuity condition $f_b(0^-) = \eta_L(E_2) f_b(0^+)$, with

$$\begin{aligned} f_b(0^+) &= -\frac{2i}{V}\big[f_2^{(\mathrm{I})}(0^+, 0^+) - f_2^{(\mathrm{II})}(0^-, 0^+)\big], \\ f_b(0^-) &= -\frac{2i}{V}\big[f_2^{(\mathrm{II})}(0^-, 0^+) - f_2^{(\mathrm{III})}(0^-, 0^-)\big]. \end{aligned} \tag{28}$$

After some calculations it is found that $B = 0$. With the use of the equation $[i(\partial_{x_1} + \partial_{x_2}) - E_2] f_2^{(\mathrm{III})}(x_1, x_2) = 0$ in subregion III, $f_2^{(\mathrm{III})}(x_1, x_2)$ becomes

$$f_2^{(\mathrm{III})}(x_1, x_2) = \frac{1}{4\pi} t_{k_1}^{(\mathrm{L})} t_{k_2}^{(\mathrm{L})} (e^{-ik_1 x_1 - ik_2 x_2} + e^{-ik_2 x_1 - ik_1 x_2}). \tag{29}$$

Finally, extending the result from the half-space to the full space using bosonic symmetry gives rise to the two-photon scattering eigenstate

$$f_2(x_1, x_2) = \frac{1}{2} \sum_{Q} f_{k_1}^{(L)}\big(x_{Q_1}\big) f_{k_2}^{(L)}\big(x_{Q_2}\big). \tag{30}$$

Here $Q = (Q_1, Q_2)$ indicates the permutation of (1,2). It corresponds to the transmission of two photons as independent particles, with the momentum of each photon conserved individually. This is because the cavity constitutes a linear system, while photon-photon interactions rely on the optical nonlinearity [24].

B. Scattering eigenstates within the right-propagating two-excitation subspace

Next, we consider the two-photon scattering eigenstates for the right-propagating incident state, where the scattering eigenstate within the two-excitation subspace is

$$\begin{aligned} |\Psi_2\rangle_R = &\iint dx_1 dx_2 f_2(x_1, x_2) \hat{c}_R^\dagger(x_1) \hat{c}_R^\dagger(x_2) |0_R, 0_a, g\rangle \\ &+ \int dx_1 f_a(x_1) \hat{c}_R^\dagger(x_1) |0_R, 1_a, g\rangle + h_a |0_R, 2_a, g\rangle \\ &+ \int dx_1 f_e(x_1) \hat{c}_R^\dagger(x_1) |0_R, 0_a, e\rangle + h_{ae} |0_R, 1_a, e\rangle. \end{aligned} \tag{31}$$

The function $f_2(x_1, x_2)$ is the probability amplitude of having two photons in the waveguide mode, $f_a(x_1)$ is the probability amplitude of one photon being in the waveguide mode with the other in the cavity mode, h_a is the probability amplitude of both excitations being in the cavity mode, $f_e(x_1)$ is the probability amplitude of having one photon in the waveguide mode and the other in the atomic excitation, and h_{ae} is the probability amplitude of having one excitation in the cavity mode and the other in the atomic excitation. From the equation $\hat{H}_R |\Psi_2\rangle_R = E_2 |\Psi_2\rangle_R$, with the eigenvalue $E_2 = k_1 + k_2$, we can obtain

$$\begin{aligned} &\big[-i\big(\partial_{x_1} + \partial_{x_2}\big) - E_2\big] f_2(x_1, x_2) \\ &\quad + \frac{V}{4}[\delta(x_1) f_a(x_2) + \delta(x_2) f_a(x_1)] = 0, \\ &\big(-i\partial_{x_1} - E_2 + \tilde{\Delta}_c\big) f_a(x_1) + \frac{g}{2} f_e(x_1) + \frac{V}{\sqrt{2}} h_a \delta(x_1) \\ &\quad + \frac{V}{2}[f_2(0, x_1) + f_2(x_1, 0)] = 0, \\ &\big(-i\partial_{x_1} - E_2 + \tilde{\Delta}_e\big) f_e(x_1) + \frac{V}{2} h_{ae} \delta(x_1) + \frac{g}{2} f_a(x_1) = 0, \\ &(2\tilde{\Delta}_c - E_2) h_a + \frac{V}{2} f_a(0) + \frac{g}{\sqrt{2}} h_{ae} = 0, \\ &(\tilde{\Delta}_c + \tilde{\Delta}_e - E_2) h_{ae} + \frac{V}{2} f_e(0) + \frac{g}{\sqrt{2}} h_a = 0. \end{aligned} \tag{32}$$

Also, $f_2(x_1, x_2)$, $f_a(x)$, and $f_e(x)$ are piecewise continuous because of the singularity of the δ function, and $f_2(0, x_1) \equiv [f_2(0^+, x_1) + f_2(0^-, x_1)]/2$, $f_2(x_1, 0) \equiv [f_2(x_1, 0^+) + f_2(x_1, 0^-)]/2$, $f_a(0) \equiv [f_a(0^+) + f_a(0^-)]/2$, and $f_e(0) \equiv [f_e(0^+) + f_e(0^-)]/2$. Waveguide-cavity-QE interactions occur at the coordinate axes $x_1 = 0$ and $x_2 = 0$ in real space, and for the region with $x_1 \neq 0$ and $x_2 \neq 0$ in the absence of interactions, $f_2(x_1, x_2)$ yields

$$\big[i\big(\partial_{x_1} + \partial_{x_2}\big) + E_2\big] f_2(x_1, x_2) = 0. \tag{33}$$

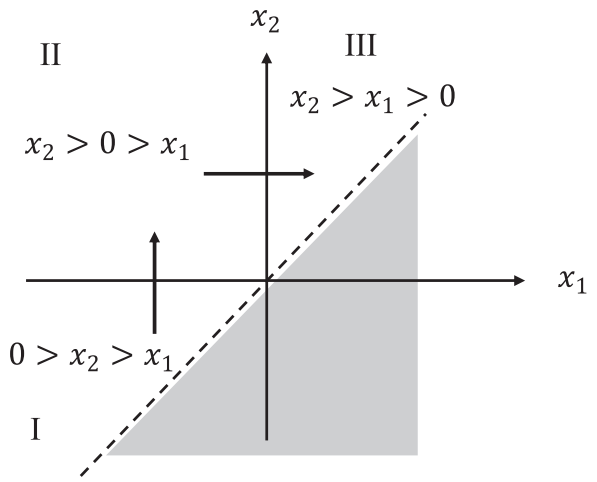

FIG. 4. The $x_2 > x_1$ region is dissected into three subregions, (I) $x_2 > x_1 > 0$, (II) $x_2 > 0 > x_1$, and (III) $0 > x_2 > x_1$, due to interactions at the coordinate axes $x_1 = 0$ and $x_2 = 0$.

The continuity conditions are necessary to calculate $f_2(x_1, x_2)$, $f_a(x_1)$, and $f_e(x_1)$. For $f_a(x_1)$ and $f_e(x_1)$, by eliminating h_a and h_{ae}, the continuity conditions become

$$\begin{aligned} &f_a(0^+) - f_a(0^-) - i\sqrt{2}M_{11}[f_a(0^+) + f_a(0^-)] \\ &\quad - i\sqrt{2}M_{12}[f_e(0^+) + f_e(0^-)] = 0, \\ &f_e(0^+) - f_e(0^-) - iM_{12}[f_a(0^+) + f_a(0^-)] \\ &\quad - iM_{22}[f_e(0^+) + f_e(0^-)] = 0, \end{aligned} \tag{34}$$

where the coefficients are

$$\begin{aligned} M_{11} &= \Gamma(\tilde{\Delta}_c + \tilde{\Delta}_e - E_2)/2\Xi, \\ M_{12} &= -\sqrt{2}\Gamma g/4\Xi, \\ M_{22} &= \Gamma(2\tilde{\Delta}_c - E_2)/2\Xi, \\ \Xi &= (2\tilde{\Delta}_c - E_2)(\tilde{\Delta}_c + \tilde{\Delta}_e - E_2) - g^2/2. \end{aligned} \tag{35}$$

To obtain $f_2(x_1, x_2)$, we first consider the half-space $x_2 > x_1$, which can be extended to the full space with the use of bosonic symmetry. In this case, the $x_2 > x_1$ region is dissected by $x_1 = 0$ and $x_2 = 0$ axes into three subregions: (I) $0 > x_2 > x_1$, (II) $x_2 > 0 > x_1$, and (III) $x_2 > x_1 > 0$, as shown in Fig. 4. In subregion I, it corresponds to the incident plane-wave field before interactions and is described by the wave function $f_2^{(\mathrm{I})}(x_1, x_2) = [h_{k_1}^{(\mathrm{R})}(x_1)h_{k_2}^{(\mathrm{R})}(x_2) + h_{k_1}^{(\mathrm{R})}(x_2)h_{k_2}^{(\mathrm{R})}(x_1)]/2$.

Through the integration of Eqs. (32) around the boundary between subregions I and II at $x_2 = 0$, we have

$$\begin{aligned} &-i\big[\tilde{f}_2^{(\mathrm{II})}(x_1, 0^+) - \tilde{f}_2^{(\mathrm{I})}(x_1, 0^-)\big] + \frac{V}{4}\tilde{f}_a(x_1) = 0, \\ &\big(-i\partial_{x_1} + \tilde{\Delta}_c\big)\tilde{f}_a(x_1) + \frac{g}{2}\tilde{f}_e(x_1) \\ &\quad + \frac{V}{2}\big[\tilde{f}_2^{(\mathrm{II})}(x_1, 0^+) + \tilde{f}_2^{(\mathrm{I})}(x_1, 0^-)\big] = 0, \\ &\big(-i\partial_{x_1} + \tilde{\Delta}_e\big)\tilde{f}_e(x_1) + \frac{g}{2}\tilde{f}_a(x_1) = 0, \end{aligned} \tag{36}$$

where $\tilde{F} = Fe^{-iE_2x_1}$ and $F = \{f_2^{(\mathrm{II})}(x_1, 0^+), f_2^{(\mathrm{I})}(x_1, 0^-), f_a(x_1), f_e(x_1)\}$, are expressed in the rotating frame. By eliminating $\tilde{f}_a(x_1)$ and $\tilde{f}_e(x_1)$, we have

$$\begin{aligned} &\left[\big(i\partial_{x_1} - \tilde{\Delta}_e\big)\left(i\partial_{x_1} - \tilde{\Delta}_c + i\frac{\Gamma}{2}\right) - \frac{g^2}{4}\right]\tilde{f}_2^{(\mathrm{II})}(x_1, 0^+) \\ &\quad = \left[\big(i\partial_{x_1} - \tilde{\Delta}_e\big)\left(i\partial_{x_1} - \tilde{\Delta}_c - i\frac{\Gamma}{2}\right) - \frac{g^2}{4}\right]\tilde{f}_2^{(\mathrm{I})}(x_1, 0^-). \end{aligned} \tag{37}$$

Because $\tilde{f}_2^{(\mathrm{I})}(x_1, 0^-) = (e^{-ik_2x_1} + e^{-ik_1x_1})/4\pi$ on the boundary of subregion I, on the boundary of subregion II,

$$\begin{aligned} \tilde{f}_2^{(\mathrm{II})}(x_1, 0^+) = \frac{1}{4\pi}\Big[&\big(t_{k_1}^{(\mathrm{R})}e^{-ik_1x_1} + t_{k_2}^{(\mathrm{R})}e^{-ik_2x_1}\big) \\ &+ c_+e^{\lambda_+x_1} + c_-e^{\lambda_-x_1}\Big], \end{aligned} \tag{38}$$

with

$$\lambda_\pm = \frac{1}{2i}\left[\tilde{\Delta}_e + \tilde{\Delta}_c - i\frac{\Gamma}{2} \pm \sqrt{\left(\tilde{\Delta}_e - \tilde{\Delta}_c + i\frac{\Gamma}{2}\right)^2 + g^2}\right]. \tag{39}$$

We should take coefficients $c_\pm$ to be zero due to the divergence in the limit $x_1 \to -\infty$. Hence, $f^{(\mathrm{II})}(x_1, 0^+) = (t_{k_1}^{(\mathrm{R})}e^{ik_2x_1} + t_{k_2}^{(\mathrm{R})}e^{ik_1x_1})/4\pi$. Under the constraint equation $[i(\partial_{x_1} + \partial_{x_2}) + E_2]f_2^{(\mathrm{II})}(x_1, x_2) = 0$ in subregion II, $f_2^{(\mathrm{II})}(x_1, x_2)$ takes the form

$$f_2^{(\mathrm{II})}(x_1, x_2) = \frac{1}{4\pi}\big(t_{k_1}^{(\mathrm{R})}e^{ik_2x_1 + ik_1x_2} + t_{k_2}^{(\mathrm{R})}e^{ik_1x_1 + ik_2x_2}\big). \tag{40}$$

Following the same procedure through the integration around the boundary of subregions II and III ($x_1 = 0$) and also introducing $\tilde{F} = Fe^{-iE_2x_2}$ and $F = \{f_2^{(\mathrm{III})}(0^+, x_2), f_2^{(\mathrm{II})}(0^-, x_2)\}$, we have

$$\begin{aligned} &\left[(i\partial_{x_2} - \tilde{\Delta}_e)\left(i\partial_{x_2} - \tilde{\Delta}_c + i\frac{\Gamma}{2}\right) - \frac{g^2}{4}\right]\tilde{f}_2^{(\mathrm{III})}(0^+, x_2) \\ &\quad = \left[(i\partial_{x_2} - \tilde{\Delta}_e)\left(i\partial_{x_2} - \tilde{\Delta}_c - i\frac{\Gamma}{2}\right) - \frac{g^2}{4}\right]\tilde{f}_2^{(\mathrm{II})}(0^-, x_2). \end{aligned} \tag{41}$$

With the use of $\tilde{f}_2^{(\mathrm{II})}(0^-, x_2) = (t_{k_1}^{(\mathrm{R})}e^{-ik_2x_2} + t_{k_2}^{(\mathrm{R})}e^{-ik_1x_2})/4\pi$, the solution on the boundary of subregion III is

$$\begin{aligned} \tilde{f}_2^{(\mathrm{III})}(0^+, x_2) = \frac{1}{4\pi}\Big[&t_{k_1}^{(\mathrm{R})}t_{k_2}^{(\mathrm{R})}(e^{-ik_2x_2} + e^{-ik_1x_2}) \\ &+ C_+e^{\lambda_+x_2} + C_-e^{\lambda_-x_2}\Big]. \end{aligned} \tag{42}$$

The coefficients $C_\pm$ are determined by continuity relations in Eqs. (34) with

$$\begin{aligned} f_a(0^-) &= \frac{4i}{V}\big[\tilde{f}_2^{(\mathrm{II})}(0^-, 0^+) - \tilde{f}_2^{(\mathrm{I})}(0^-, 0^-)\big], \\ f_a(0^+) &= \frac{4i}{V}\big[\tilde{f}_2^{(\mathrm{III})}(0^+, 0^+) - \tilde{f}_2^{(\mathrm{II})}(0^-, 0^+)\big], \\ f_e(0^-) &= \frac{8i}{gV}\big[\big(i\partial_{x_1} - \tilde{\Delta}_c + i\Gamma/2\big)\tilde{f}_2^{(\mathrm{II})}(x_1, 0^+) \\ &\quad - \big(i\partial_{x_1} - \tilde{\Delta}_c - i\Gamma/2\big)\tilde{f}_2^{(\mathrm{I})}(x_1, 0^-)\big]\,|_{x_1 \to 0^-}, \end{aligned}$$

$$f_e(0^+) = \frac{8i}{gV}\big[\big(i\partial_{x_2} - \tilde{\Delta}_c + i\Gamma/2\big)\tilde{f}_2^{(\mathrm{III})}(0^+, x_2) - \big(i\partial_{x_2} - \tilde{\Delta}_c - i\Gamma/2\big)\tilde{f}_2^{(\mathrm{II})}(0^-, x_2)\big]\,|_{x_2\to 0^+}\,. \quad (43)$$

Then out of the rotating frame in Eq. (42) we have

$$f_2^{(\mathrm{III})}(0^+, x_2) = \frac{1}{4\pi}\big[t_{k_1}^{(\mathrm{R})} t_{k_2}^{(\mathrm{R})}(e^{ik_1x_2} + e^{ik_2x_2}) + C_+ e^{(\lambda_+ + iE_2)x_2} + C_- e^{(\lambda_- + iE_2)x_2}\big]. \quad (44)$$

With the use of the equation $[i(\partial_{x_1} + \partial_{x_2}) + E_2]f_2^{(\mathrm{III})}(x_1, x_2) = 0$ in subregion III, $f_2^{(\mathrm{III})}(x_1, x_2)$ becomes

$$f_2^{(\mathrm{III})}(x_1, x_2) = \frac{1}{4\pi} t_{k_1}^{(\mathrm{R})} t_{k_2}^{(\mathrm{R})}(e^{ik_1x_2 + ik_2x_1} + e^{ik_1x_1 + ik_2x_2}) + \frac{e^{iE_2x_2}}{4\pi}[C_+ e^{\lambda_+(x_2 - x_1)} + C_- e^{\lambda_-(x_2 - x_1)}]. \quad (45)$$

Finally, according to bosonic symmetry, the result can be extended from the half-space to the full space, where the two-photon scattering eigenstate becomes

$$f_2(x_1, x_2) = \frac{1}{2}\Big[\sum_Q f_{k_1}^{(R)}(x_{Q_1}) f_{k_2}^{(R)}(x_{Q_2}) + \sum_{PQ} C^{(2)}_{k_{P_1}, k_{P_2}}(x_{Q_1}, x_{Q_2})\theta(x_{Q_1})\Big], \quad (46)$$

where

$$C^{(2)}_{k_{P_1}, k_{P_2}}(x_{Q_1}, x_{Q_2}) = \frac{e^{iE_2x_{Q_2}}}{4\pi}[C_+ e^{\lambda_+|x_{Q_2} - x_{Q_1}|} + C_- e^{\lambda_-|x_{Q_2} - x_{Q_1}|}]\theta(x_{Q_2} - x_{Q_1}). \quad (47)$$

Here $P = (P_1, P_2)$ and $Q = (Q_1, Q_2)$ indicate the permutations of (1,2) to account for the bosonic symmetry of the wave function. The first term of $f_2(x_1, x_2)$ corresponds to the transmission of two photons as independent particles, with the momentum of each photon conserved individually. The second term indicates the formation of a two-body bound state, which is induced by the nonlinear cavity-QE interactions. The momentum of each photon in the bound state is not conserved, while the total momentum is conserved [29]. The bound-state term shows an exponential decay in the relative coordinate $|x_2 - x_1|$, with two characteristic binding strengths $\lambda_\pm$. Because the interaction is spatially confined, energy and momentum can be exchanged and redistributed between the photons (with the constraint of fixed total energy), enabling the formation of photon-photon correlations.

To manifest the effective spatial interaction between photons, we consider the asymptotic behavior (away from the cavity and with $x_1 > 0$, $x_2 > 0$) of the two-photon scattering eigenstate in the central and relative coordinates, i.e., $x_c \equiv (x_1 + x_2)/2$, $x \equiv x_1 - x_2$, which is

$$f_2(x_c, x) = \frac{e^{iE_2x_c}}{2\pi}\big[t_{k_1}^{(\mathrm{R})} t_{k_2}^{(\mathrm{R})} \cos\Delta_1 x + \frac{1}{2} e^{iE_2|x|/2}(C_+ e^{\lambda_+|x|} + C_- e^{\lambda_-|x|})\big], \quad (48)$$

with $\Delta_1 \equiv k_1 - E_2/2 = (k_1 - k_2)/2$. Here the relative coordinate x is equivalent to a time delay τ between the two scattered photons [42]. In order to study the two-photon bunch or antibunch after scattering, we present comparisons between $|f_2(x_c, x)|^2$ and the case without cavity-QE interaction, which is denoted by $\tilde{f}_2(x_c, x) = \frac{e^{iE_2x_c}}{2\pi} t_{k_1}^{(\mathrm{R})} t_{k_2}^{(\mathrm{R})} \cos\Delta_1 x$, in Fig. 5. For $x = 0$, the ratio between the two cases reaches the maximum around $E_2 = 0$ and $\Delta_1 = 0$, as shown in Fig. 5(a). The maximum is larger than 1, which implies that the eigenstate is not a product state but the bound state forms after scattering. Moreover, we plot $|f_2(x_c, x)|^2$ as a function of x under the condition $E_2 = \Delta_1 = 0$ in Fig. 5(b). It shows a cusp at $x = 0$, indicating bunched photons, and an exponentially decaying feature in x with a half-width of $2/(\kappa + \Gamma)$ in space. Therefore, when Δ_1 is gradually increased from zero to $(\kappa + \Gamma)/4$, the peak at $x = 0$ decreases from its maximum to zero. The transmitted photons will change from bunching to antibunching. For example, in the case of $\Delta_1 = -0.5\kappa$ in Fig. 5(c), the peak is larger than that in the case without interaction, while in the case of $\Delta_1 = -1.25\kappa$ in Fig. 5(d), the peak is completely depleted.

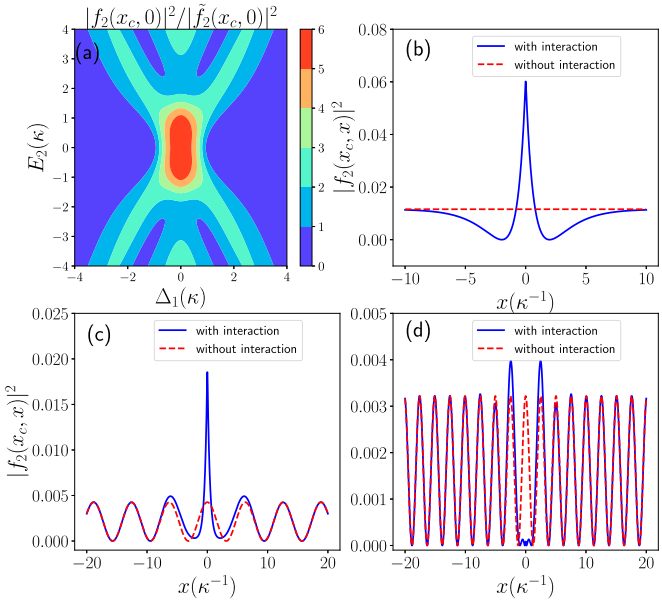

FIG. 5. (a) Plot of $|f_2(x_c, 0)|^2/|\tilde{f}_2(x_c, 0)|^2$ as a function of E_2 and Δ_1 (in units of κ). (b)–(d) Plots of $|f_2(x_c, x)|^2$ as a function of x (in units of κ^{-1}) for different detunings: (b) $\Delta_1 = 0$, (c) $\Delta_1 = -0.5\kappa$, and (d) $\Delta_1 = -1.25\kappa$. Dashed lines indicate the interaction-free case, while solid lines indicate interactions of right-propagating photons in the system. The other parameters are $\Delta_c = 0$, $\Delta_e = 0$, $g = 2\kappa$, $\gamma = 0.1\kappa$, and $\Gamma = 4\kappa$.

V. NONRECIPROCAL PHOTON BLOCKADE

Photon blockade, a purely quantum effect, has been utilized to achieve tunable nonclassical signals [43,44]. Thus, nonreciprocal photon blockade devices, together with other quantum one-way devices, are important elements in quantum metrology [45], quantum simulations [46], and QIP [47–49]. Nonreciprocal photon blockade has been investigated in the nonlinear cavity system based on the anharmonicity of the spectrum in the spinning system [50–53]. Here we focus on the nonreciprocal photon blockade in the chiral waveguide

system for incident optical pulses since in optical devices and QIP the signals are typically pulses. In this chiral system, for the left-propagating photons, the cavity serves as a linear absorber, and only the classical features of light appear; that is, the transmission is blocked at the resonance frequency. However, the quantum nonlinearity for right-propagating photons can induce photon-photon interactions, i.e., the formation of a bound state. Then, the quantum features, such as photon blockade, can emerge. The pulsed two-photon incident states are described by the wave packets [54]

$$\left|\psi_j^{(2)}\right\rangle = \frac{1}{\sqrt{2}}\left[\int dk\alpha(k)|k\rangle_j\right]^2 \quad (j = R, L), \tag{49}$$

which are the direct generalization of the single-photon wave packet in Eq. (15). Then, the two-photon output states can be derived as

$$\begin{aligned}\left|\varphi_j^{(2)}\right\rangle &= \iint dk_1 dk_2 \frac{1}{\sqrt{2}}\alpha(k_1)\alpha(k_2)\left|\phi_j^{(2)}(k_1,k_2)\right\rangle,\\ \left|\phi_j^{(2)}(k_1,k_2)\right\rangle &= \frac{1}{2}\iint dx_1 dx_2 t_{k_1,k_2}^{(j)}(x_1,x_2)\hat{c}_j^\dagger(x_1)\hat{c}_j^\dagger(x_2)|0\rangle,\end{aligned} \tag{50}$$

where the coefficients are

$$\begin{aligned}t_{k_1,k_2}^{(L)}(x_1,x_2) &= t_{k_1}^{(L)}t_{k_2}^{(L)}h_{k_1}^{(L)}(x_1)h_{k_2}^{(L)}(x_2) + k_1 \leftrightarrow k_2,\\ t_{k_1,k_2}^{(R)}(x_1,x_2) &= t_{k_1}^{(R)}t_{k_2}^{(R)}h_{k_1}^{(R)}(x_1)h_{k_2}^{(R)}(x_2)\\ &\quad + B_{k_1,k_2}^{(2)}(x_1,x_2) + k_1 \leftrightarrow k_2,\\ B_{k_1,k_2}^{(2)}(x_1,x_2) &= C_{k_1,k_2}^{(2)}(x_1,x_2) + C_{k_1,k_2}^{(2)}(x_2,x_1).\end{aligned} \tag{51}$$

The two-photon transmission probabilities are defined as

$$P_j^{(2)} = \iint dk_1 dk_2 \frac{1}{2!}\left|{}_j\langle k_1 k_2|\varphi_j^{(2)}\rangle\right|^2. \tag{52}$$

For left-propagating photons, due to the absence of photon-photon interactions, the photons transmit independently, and the probability is

$$\begin{aligned}P_L^{(2)} &= \iint dk_1 dk_2 \left|t_L^{(2)}(k_1,k_2)\right|^2,\\ t_L^{(2)}(k_1,k_2) &= \alpha(k_1)\alpha(k_2)t_{k_1}^{(L)}t_{k_2}^{(L)}.\end{aligned} \tag{53}$$

However, for right-propagating photons, the transmission probability becomes

$$\begin{aligned}P_R^{(2)} &= \iint dk_1 dk_2 \left|t_R^{(2)}(k_1,k_2) + B(k_1,k_2)\right|^2,\\ t_R^{(2)}(k_1,k_2) &= \alpha(k_1)\alpha(k_2)t_{k_1}^{(R)}t_{k_2}^{(R)},\\ B(k_1,k_2) &= -\frac{1}{4\pi}\sum_{m=+,-}\left(\frac{1}{\lambda_m + ik_1} + \frac{1}{\lambda_m + ik_2}\right)\\ &\quad \times \int dk\alpha(k)\alpha(k_1+k_2-k)C_m(k,k_1+k_2-k),\end{aligned} \tag{54}$$

which is determined by the interference between the plane-wave term $t_R^{(2)}(k_1,k_2)$ and the bound-state term $B(k_1,k_2)$.

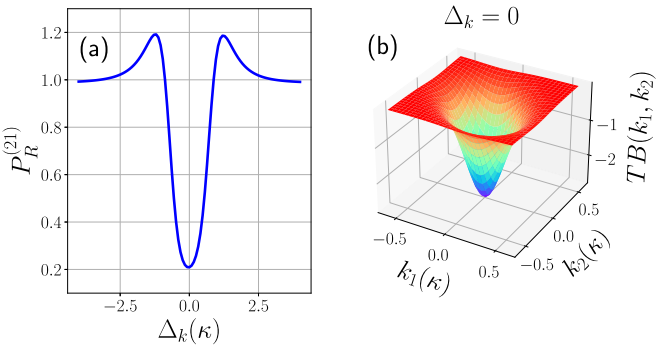

FIG. 6. (a) Photon blockade strength $P_R^{(21)}$ in the right direction as a function of Δ_k (in units of κ), where a clear photon blockade is exhibited on resonance, i.e., $\Delta_k = 0$. (b) The integrand function $TB(k_1,k_2)$ of the interference term as a function of k_1 and k_2 (in units of κ). The other parameters are $\Delta_c = 0$, $\Delta_e = 0$, $g = 2\kappa$, $\gamma = 0.1\kappa$, and $\Gamma = 4\kappa$.

To quantify strengths of photon blockade in two directions, we follow the definition given in Refs. [27,28],

$$P_i^{(21)} = P_i^{(2)}/T_i^2, \tag{55}$$

which indicates the conditional probability for transmitting a second photon given that the first photon has already been transmitted $P_i^{(2)}/T_i$, normalized by the single-photon transmission probability T_i. The left-propagating photons transmit independently. There is no photon blockade, and $P_L^{(21)} = 1$. Hence, the statistics of incident photons cannot be altered in the left direction. In contrast, photons in the right-propagating direction can exhibit the photon blockade at $\Delta_k = 0$, as shown in Fig. 6(a). In combination with the single-photon transparency at $\Delta_k = 0$, this means that the single-photon transparency does not carry over to the two-photon case. Such a photon blockade regulates the flow of photons in an ordered manner, enabling the capability to generate a unidirectional single-photon source on demand by sending coherent states into such a system.

To understand the origin of photon blockade, the interference between plane-wave and bound-state terms plays a key role. From the two-photon transmission probability $P_R^{(2)}$ in Eq. (54), the integrand function of interference term can be written as

$$TB(k_1,k_2) = t_R^{(2)}(k_1,k_2)B^*(k_1,k_2) + \text{c.c.} \tag{56}$$

Figure 6(b) shows that when the center frequency of incident photons is resonant with cavity frequency, $TB(k_1,k_2)$ is always negative, suppressing the overall two-photon transmission. The cause of the observed photon blockade is thus the destructive interference between two transmission pathways: passing as independent particles or as a composite particle in the form of a bound state. In addition, the bound-state effect in photonic transport relies on the width of incident wave packet because photons should coincide at the site of the cavity-QE system. In the limit of $\sigma \to 0$, which is the ideal condition of single-photon transmission, as shown in Fig. 2, the system becomes transparent to the incoming photons due

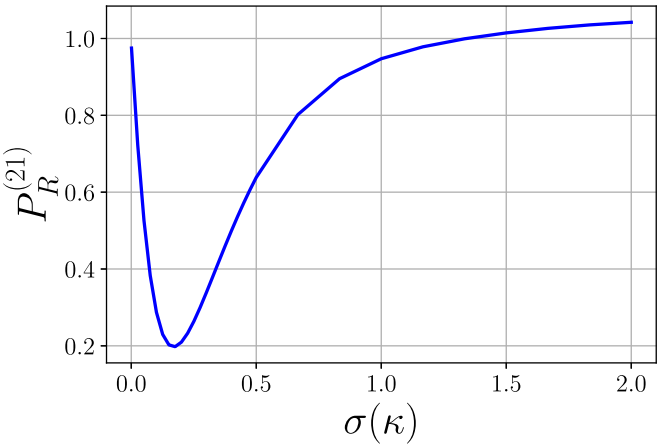

FIG. 7. Photon blockade strength $P_R^{(21)}$ in the right direction as a function of spectral width σ (in units of κ). The other parameters are $\Delta_c = 0$, $\Delta_e = 0$, $g = 2\kappa$, $\gamma = 0.1\kappa$, $\Delta_k = 0$, and $\Gamma = 4\kappa$.

to the electromagnetically-induced-transparency-like effect. However, the probability of coincidence approaches zero, and the system-mediated photon-photon interactions tend to vanish, inhibiting the effective formation of the bound state. Thus, in the $\sigma \to 0$ limit, $P_R^{(21)} \to 1$, as shown in Fig. 7.

VI. CONCLUSIONS

To conclude, we have studied the nonreciprocal properties of single-photon and two-photon transmissions in the chiral waveguide-cavity-QE system. Due to the chiral interactions between the cavity and QE, photons in the left direction couple to only the cavity, which serves as a linear absorber, while photons in the right direction couple to the cavity-QE system that forms a nonlinear optical system. In the single-photon dynamics, when the center frequency of the incident wave packet is resonant with cavity frequency, the left-propagating photon is absorbed by the cavity, and transmission is blocked. In comparison, in the right direction when the center frequency is on resonance, which is right positioned between the Rabi splittings induced by cavity-QE interactions, the single-photon transmission shows a sharp peak. In the two-photon dynamics, photon-photon interactions depend on optical nonlinearities. Hence in the left direction, the coupling to a linear cavity does not alter the statistics of incident photons, but the photon blockade is achieved in the right direction at the single-photon transparency window, opening up a new route to achieve a one-way single-photon source. Moreover, the strength of photon-photon interactions depends on the width of the incident wave packet because of the coincidence. In the narrow-width limit, interactions are significantly decreased, suppressing the effects of photon blockade.

[1] D. E. Chang, J. S. Douglas, A. González-Tudela, C.-L. Hung, and H. J. Kimble, Colloquium: Quantum matter built from nanoscopic lattices of atoms and photons, Rev. Mod. Phys. **90**, 031002 (2018).

[2] A. V. Kuhlmann, J. H. Prechtel, J. Houel, A. Ludwig, D. Reuter, A. D. Wieck, and R. J. Warburton, Transform-limited single photons form a single quantum dot, Nat. Commun. **6**, 8204 (2015).

[3] T. Nieddu, V. Gokhroo, and S. N. Chormaic, Optical nanofibres and neutral atoms, J. Opt. **18**, 053001 (2016).

[4] R. Uppu, L. Midolo, X. Zhou, J. Carolan, and P. Lodahl, Quantum-dot-based deterministic photon-emitter interfaces for scalable photonic quantum technology, Nat. Nanotechnol. **16**, 1308 (2021).

[5] P. Senellart, G. Solomon, and A. White, High-performance semiconductor quantum-dot single-photon sources, Nat. Nanotechnol. **12**, 1026 (2017).

[6] R. Uppu, F. T. Pedersen, Y. Wang, C. T. Olesen, C. Papon, X. Zhou, L. Midolo, S. Scholz, A. D. Wieck, A. Ludwig, and P. Lodahl, Scalable integrated single-photon source, Sci. Adv. **6**, eabc8268 (2020).

[7] P. Lodahl, S. Mahmoodian, S. Stobbe, A. Rauschenbeutel, P. Schneeweiss, J. Volz, H. Pichler, and P. Zoller, Chiral quantum optics, Nature (London) **541**, 473 (2017).

[8] J. Petersen, J. Volz, and A. Rauschenbeutel, Chiral nanophotonic waveguide interface based on spin-orbit interaction of light, Science **346**, 67 (2014).

[9] D. R. Abujetas and J. A. Sánchez-Gil, Spin angular momentum of guided light induced by transverse confinement and intrinsic helicity, ACS Photonics **7**, 534 (2020).

[10] R. Jones, G. Buonaiuto, B. Lang, I. Lesanovsky, and B. Olmos, Collectively Enhanced Chiral Photon Emission from an Atomic Array near a Nanofiber, Phys. Rev. Lett. **124**, 093601 (2020).

[11] P. Solano, J. A. Grover, J. E. Hoffman, S. Ravets, F. K. Fatemi, L. A. Orozco, and S. L. Rolston, Optical nanofibers: A new platform for quantum optics, Adv. At. Mol. Opt. Phys. **66**, 439 (2017).

[12] I. Söllner, S. Mahmoodian, S. L. Hansen, L. Midolo, A. Javadi, G. Kiršanskė, T. Pregnolato, H. El-Ella, E. H. Lee, J. D. Song, S. Stobbe, and P. Lodahl, Deterministic photon-emitter coupling in chiral photonic circuits, Nat. Nanotechnol. **10**, 775 (2015).

[13] K. Xia, G. Lu, G. Lin, Y. Cheng, Y. Niu, S. Gong, and J. Twamley, Reversible nonmagnetic single-photon isolation using unbalanced quantum coupling, Phys. Rev. A **90**, 043802 (2014).

[14] L. Tang, J. Tang, W. Zhang, G. Lu, H. Zhang, Y. Zhang, K. Xia, and M. Xiao, On-chip chiral single-photon interface: Isolation and unidirectional emission, Phys. Rev. A **99**, 043833 (2019).

[15] K. Koshino, K. Inomata, Z. Lin, Y. Nakamura, and T. Yamamoto, Theory of microwave single-photon detection using an impedance-matched Λ system, Phys. Rev. A **91**, 043805 (2015).

[16] K. Koshino, S. Ishizaka, and Y. Nakamura, Deterministic photon-photon $\sqrt{\text{SWAP}}$ gate using a λ system, Phys. Rev. A **82**, 010301(R) (2010).

[17] L. M. Duan and H. J. Kimble, Scalable Photonic Quantum Computation through Cavity-Assisted Interactions, Phys. Rev. Lett. **92**, 127902 (2004).

[18] E. J. Lenferink, G. Wei, and N. P. Stern, Coherent optical nonreciprocity in axisymmetric resonators, Opt. Express **22**, 16099 (2014).

[19] E. Will, L. Masters, A. Rauschenbeutel, M. Scheucher, and J. Volz, Coupling a Single Trapped Atom to a Whispering-Gallery-Mode Microresonator, Phys. Rev. Lett. **126**, 233602 (2021).

[20] D. M. Cano, H. R. Haakh, and N. Rotenberg, Chiral emission into nanophotonic resonators, ACS Photonics **6**, 961 (2019).

[21] C. Junge, D. O'shea, J. Volz, and A. Rauschenbeutel, Strong Coupling between Single Atoms and Nontransversal Photons, Phys. Rev. Lett. **110**, 213604 (2013).

[22] C. Z. Chai, H. Q. Zhao, H. X. Tang, G. C. Guo, C. L. Zou, and C. H. Dong, Non-reciprocity in high-Q ferromagnetic microspheres via photonic spin-orbit coupling, Laser Photonics Rev. **14**, 1900252 (2020).

[23] D. Hallett, A. P. Foster, D. Whittaker, M. S. Skolnick, and L. R. Wilson, Engineering chiral light-matter interactions in a waveguide-coupled nanocavity, ACS Photonics **9**, 706 (2022).

[24] D. E. Chang, V. Vuetić, and M. D. Lukin, Quantum nonlinear optics—Photon by photon, Nat. Photonics **8**, 685 (2014).

[25] O. Firstenberg, T. Peyronel, Q. Y. Liang, A. V. Gorshkov, M. D. Lukin, and V. Vuletić, Attractive photons in a quantum nonlinear medium, Nature (London) **502**, 71 (2013).

[26] R. J. Thompson, G. Rempe, and H. J. Kimble, Observation of Normal-Mode Splitting for an Atom in an Optical Cavity, Phys. Rev. Lett. **68**, 1132 (1992).

[27] H. Zheng, D. J. Gauthier, and H. U. Baranger, Cavity-Free Photon Blockade Induced by Many-Body Bound States, Phys. Rev. Lett. **107**, 223601 (2011).

[28] H. Zheng, D. J. Gauthier, and H. U. Baranger, Strongly correlated photons generated by coupling a three- or four-level system to a waveguide, Phys. Rev. A **85**, 043832 (2012).

[29] J. T. Shen and S. Fan, Strongly Correlated Two-Photon Transport in a One-Dimensional Waveguide Coupled to a Two-Level System, Phys. Rev. Lett. **98**, 153003 (2007).

[30] D. Roy, C. M. Wilson, and O. Firstenberg, Strongly interacting photons in one-dimensional continuum, Rev. Mod. Phys. **89**, 021001 (2017).

[31] D. Roy, Two-Photon Scattering by a Driven Three-Level Emitter in a One-Dimensional Waveguide and Electromagnetically Induced Transparency, Phys. Rev. Lett. **106**, 053601 (2011).

[32] J. T. Shen and S. Fan, Theory of single-photon transport in a single-mode waveguide. I. Coupling to a cavity containing a two-level atom, Phys. Rev. A **79**, 023837 (2009).

[33] J. T. Shen and S. Fan, Theory of single-photon transport in a single-mode waveguide. II. Coupling to a whispering-gallery resonator containing a two-level atom, Phys. Rev. A **79**, 023838 (2009).

[34] C. W. Gardiner and M. J. Collett, Input and output in damped quantum systems: Quantum stochastic differential equations and the master equation, Phys. Rev. A **31**, 3761 (1985).

[35] Y. Zhang and B. Zou, Effects of non-δ coupling between one-dimensional waveguides and side optical cavities, Phys. Rev. A **89**, 063815 (2014).

[36] J. T. Shen and S. Fan, Strongly correlated multiparticle transport in one dimension through a quantum impurity, Phys. Rev. A **76**, 062709 (2007).

[37] Y. M. Hao, G. W. Lin, K. Xia, X. M. Lin, Y. P. Niu, and S. Q. Gong, Quantum controlled-phase-flip gate between a flying optical photon and a Rydberg atomic ensemble, Sci. Rep. **5**, 10005 (2015).

[38] S. Das, A. Grankin, I. Iakoupov, E. Brion, J. Borregaard, R. Boddeda, I. Usmani, A. Ourjoumtsev, P. Grangier, and A. S. Sørensen, Photonic controlled-phase-gates through Rydberg blockade in optical cavities, Phys. Rev. A **93**, 040303(R) (2016).

[39] A. C. J. Wade, M. Mattioli, and K. Mølmer, Single-atom single-photon coupling facilitated by atomic-ensemble dark-state mechanisms, Phys. Rev. A **94**, 053830 (2016).

[40] J. Vaneecloo, S. Garcia, and A. Ourjoumtsev, Intracavity Rydberg Superatom for Optical Quantum Engineering: Coherent Control, Single-Shot Detection, and Optical π Phase Shift, Phys. Rev. X **12**, 021034 (2022).

[41] T. Stolz, H. Hegels, M. Winter, B. Röhr, Y. F. Hsiao, L. Husel, G. Rempe, and S. Dürr, Quantum-Logic Gate between Two Optical Photons with an Average Efficiency Above 40%, Phys. Rev. X **12**, 021035 (2022).

[42] I. C. Hoi, T. Palomaki, J. Lindkvist, G. Johansson, P. Delsing, and C. M. Wilson, Generation of Nonclassical Microwave States Using an Artificial Atom in 1D Open Space, Phys. Rev. Lett. **108**, 263601 (2012).

[43] D. E. Chang, A. S. Sørensen, E. A. Demler, and M. D. Lukin, A single-photon transistor using nanoscale surface plasmons, Nat. Phys. **3**, 807 (2007).

[44] A. Kubanek, A. Ourjoumtsev, I. Schuster, M. Koch, P. W. H. Pinkse, K. Murr, and G. Rempe, Two-Photon Gateway in One-Atom Cavity Quantum Electrodynamics, Phys. Rev. Lett. **101**, 203602 (2008).

[45] F. Lecocq, L. Ranzani, G. A. Peterson, K. Cicak, A. Metelmann, S. Kotler, R. W. Simmonds, J. D. Teufel, and J. Aumentado, Microwave Measurement beyond the Quantum Limit with a Nonreciprocal Amplifier, Phys. Rev. Appl. **13**, 044005 (2020).

[46] I. M. Georgescu, S. Ashhab, and F. Nori, Quantum simulation, Rev. Mod. Phys. **86**, 153 (2014).

[47] K. M. Sliwa, M. Hatridge, A. Narla, S. Shankar, L. Frunzio, R. J. Schoelkopf, and M. H. Devoret, Reconfigurable Josephson Circulator/Directional Amplifier, Phys. Rev. X **5**, 041020 (2015).

[48] F. Lecocq, L. Ranzani, G. A. Peterson, K. Cicak, R. W. Simmonds, J. D. Teufel, and J. Aumentado, Nonreciprocal Microwave Signal Processing with a Field-Programmable Josephson Amplifier, Phys. Rev. Appl. **7**, 024028 (2017).

[49] L. M. de Lépinay, E. Damskägg, C. F. Ockeloen-Korppi, and M. A. Sillanpää, Realization of Directional Amplification in a Microwave Optomechanical Device, Phys. Rev. Appl. **11**, 034027 (2019).

[50] R. Huang, A. Miranowicz, J. Q. Liao, F. Nori, and H. Jing, Nonreciprocal Photon Blockade, Phys. Rev. Lett. **121**, 153601 (2018).

[51] X. W. Xu, Y. Li, B. Li, H. Jing, and A. X. Chen, Nonreciprocity via Nonlinearity and Synthetic Magnetism, Phys. Rev. Appl. **13**, 044070 (2020).

[52] B. Li, R. Huang, X. W. Xu, A. Miranowicz, and H. Jing, Nonreciprocal unconventional photon blockade in a spinning optomechanical system, Photonics Res. **7**, 630 (2019).

[53] H. Z. Shen, Q. Wang, J. Wang, and X. X. Yi, Nonreciprocal unconventional photon blockade in a driven dissipative cavity with parametric amplification, Phys. Rev. A **101**, 013826 (2020).

[54] P. P. Rohde, W. Mauerer, and C. Silberhorn, Spectral structure and decompositions of optical states and their applications, New J. Phys. **9**, 91 (2007).